Toward Real-time Solar Content-based Image Retrieval

Rafał Grycuk[1][0000−0002−3097−985X], Giorgio De Magistris[2][0000−0002−3076−4509], Christian Napoli[2,3][0000−0002−3336−5853], and Rafał Scherer[1][0000−0001−9592−262X]

[1] Czestochowa University of Technology, al. Armii Krajowej 36, Czestochowa, Poland
{rafal.grycuk,rafal.scherer}@pcz.pl
[2] Department of Computer, Control and Management Engineering, Sapienza University of Rome
{cnapoli,demagistris}@diag.uniroma1.it
[3] Institute for Systems Analysis and Computer Science, Italian National Research Council

Abstract. We present a new approach for real-time retrieval and classification of solar images using a proposed sector-based image hashing technique. To this end, we generate intermediate hand-crafted features from automatically detected active regions in the form of layer-sector-based descriptors. Additionally, we employ a small fully-connected autoencoder to encode and finally obtain the concise Layer-Sector Solar Hash. By reducing the amount of data required to describe the Sun images, we achieve almost real-time retrieval speed of similar images to the query image. Since solar AIA images are not labeled, for the purposes of the presented test experiments, we consider images produced within a short time frame (typically up to several hours) to be similar. This approach has several potential applications, including searching, classifying, and retrieving solar flares, which are of critical importance for many aspects of life on Earth.

1 Introduction

The Solar Dynamics Observatory (SDO) was launched by NASA in 2010 as a part of the Living with a Star program with the aim of providing data to study the interconnected Sun-Earth system and how the Sun impacts life on Earth. The Sun's activity, such as massive electromagnetic storms, can negatively affect various technologies including electronics, navigation systems, and electric power grids. Solar activity, which is influenced by the sunspot cycle and other transient aperiodic processes, plays a significant role in creating space weather that affects both space- and ground-based technologies, as well as the Earth's atmosphere. Furthermore, the Sun's behavior is partially responsible for climate fluctuations on a scale of centuries and longer. Comprehending and forecasting the sunspot cycle continues to be a significant scientific challenge, with far-reaching consequences for space science and our understanding of magnetohydrodynamic phenomena in the Solar System and on Earth.

ICCS Camera Ready Version 2024
To cite this paper please use the final published version:
DOI: 10.1007/978-3-031-63749-0_8

The SDO is a 3-axis stabilized spacecraft equipped with three main sensoric instruments, one of which is the Atmospheric Imaging Assembly (AIA). AIA continuously captures full-disk observations of the solar chromosphere and corona in seven extreme ultraviolet (EUV) channels, producing high-resolution images with a 12-second cadence at 4096×4096 pixels. The commencement of the SDO program enabled the analysis of solar activity, despite the challenge of dealing with big data. SDO generates around 70 thousand images every day, which makes it impossible to manually search and annotate this vast collection of images. Additionally, the repetitiveness and monotony of these images make the annotation process even more difficult for humans. The images captured by the SDO are quite similar to one another, making it challenging to describe them using general-purpose visual features. Additionally, the images are only labeled by their timestamp, which further adds to the difficulty in analyzing and categorizing them.

For our research, we utilize a 4K resolution dataset that has been prepared by Kucuk et al. [19] specifically for image retrieval purposes. This dataset comprises hundreds of thousands of full-disk images of the Sun, with temporal and spatial event features included in the records. Such large datasets are difficult to search and detect changes anomalies [9, 17].

Traditionally, hand-crafted features have been used to classify or predict the state of the Sun from its images. For instance, Banda et al. [2] identified ten distinct image parameters that are the best representation of the Solar state when extracted from Solar full-disk images. These parameters are also present in the dataset we use. In [4], the Lucene retrieval engine was modified to retrieve solar images based on descriptive solar features developed in [3]. These features have also been utilized by Boubrahimi et al. in [6] and Ma et al. in [20] to forecast solar event trajectories.

Our paper introduces a solar hash designed to locate similar solar images from a vast collection of solar images. We employ a fully-connected autoencoder that operates on preprocessed solar full-disk projections. Our emphasis is on optimizing the retrieval process, and our proposed method outperforms existing methods in terms of speed and accuracy. The proposed solar hashes are key to achieving faster retrieval times. It is worth noting that direct full-disk solar image hashing is computationally demanding (for one year period approx 10 days), which was the primary motivation for our work.

The rest of the paper is organized as follows. In Section 2 we describe shortly other content-based image retrieval methods. The proposed method is described in Section 3. The experiments are described in Section 4. Section 5 concludes the paper.

2 Related Works

The article [1] details a system for content-based image retrieval that covers the entire disk. The authors experimented with eighteen image similarity measures and a range of image features, resulting in one hundred and eighty unique com-

ICCS Camera Ready Version 2024
To cite this paper please use the final published version:
DOI: 10.1007/978-3-031-63749-0_8

binations. Through these experiments, the authors identified suitable metrics for comparing solar images, which can aid in the retrieval and classification of various phenomena. The article referenced as [3] outlines a segmentation method for full-disk SDO images, where sub-images are created based on a 64×64 grid. Ten parameters are then calculated for each sub-image, including entropy, fractal dimension, mean intensity, third and fourth moments, relative smoothness, standard deviation of intensity, Tamura contrast, Tamura directionality, and uniformity.

In [4], the retrieval of solar images is performed using Lucene, a versatile retrieval engine. Each image is considered a distinct document, comprising 64 elements (rows of each image). To locate similar solar events, wild-card characters are used in the query strings. In [5], the effectiveness of the Lucene engine is compared to distance-based image retrieval approaches, but no clear winner is identified. The tested methods each exhibit advantages and drawbacks in terms of accuracy, speed, and suitability. The balance between accuracy and speed is considerable, with retrieval times of several minutes being necessary for precise outcomes. In [14], a sparse model representation was introduced for solar images, utilizing the approach from [21]. The proposed method surpassed previous solar image retrieval techniques in both accuracy and speed.

In [16], certain solar image parameters are selected to monitor various solar events across images with a 6-minute interval. In [15], sparse codes for AIA images are also utilized, with ten texture-based image parameters being employed to generate the code. The parameters are determined for regions identified by a 64×64 grid for nine wavelengths. A dictionary of k elements is learned for each wavelength, and a sparse representation is subsequently calculated. In order to address the issue of dimensionality that impacts solar data, the researchers employed the Minkowski norm and carefully selected an appropriate value for the parameter p. As a result of their efforts, they were able to utilize a 256-dimensional descriptor that demonstrated both efficiency and accuracy, surpassing previous methodologies. In recent years, significant progress has been made in image retrieval using learned semantic hashes [18]. The objective of semantic hashing [23] is to generate concise vectors that capture the semantic information of objects. By searching for similar hashes, we can quickly retrieve similar objects, a process that is considerably faster and requires less memory than direct manipulation of the objects themselves. Generating hashes from high-resolution full-disk solar images would not be feasible due to the sheer size of the image collections. As a result, we have devised a new rapid binary hash based on the engineered features we refer to as intermediate descriptors throughout this paper.

3 Proposed Method for Solar Image Hashing

In this section, we introduce an innovative approach to create a hash for solar images. This hash can be used later on to retrieve solar images from vast collections of solar image datasets. We obtained the solar images from the Solar

ICCS Camera Ready Version 2024
To cite this paper please use the final published version:
DOI: 10.1007/978-3-031-63749-0_8

Dynamics Observatory (SDO), which were refined and released through a Web API by [19]. Although the API provides several resolutions, we opted for a resolution of 2048×2048. We performed evaluation study in order to determine the best resolution. The results, determine 2048×2048 as the best one. The algorithm we present comprises three primary stages: computing the descriptor of the solar image, hashing the descriptor, and retrieving the solar image.

3.1 Calculating Solar Image Descriptor

At this stage, we input a solar image and generate a corresponding solar image descriptor as output. After extensive research, we concluded that the most suitable image resolution to use is 2048×2048. Hence, we obtain a solar image descriptor as output by providing a solar image as input at a resolution of 2048×2048. The input image is obtained from the SDO's AIA (Atmospheric Imaging Assembly) instrument. The brighter areas visible in the input image correspond to Active Regions (ARs), which are of great significance in studying solar flares. These flares pose a significant risk to the safety of power grids, satellites, and other electronic devices situated in Earth's orbit or on its surface, making the study of ARs particularly important.

Active Regions (ARs) can exhibit a wide range of shapes and positions relative to the SDO telescope that can change as a result of the Sun's rotational movement. The first stage of the proposed method involves detecting and describing the shapes and positions of ARs. This stage comprises a sequence of steps, starting with the conversion of the image from RGB to grayscale to reduce the number of color channels from three to one. Subsequently, the pixel intensity values are in the range of $[0 : 255]$. A Gaussian blur filter, a widely used image filter, is then applied to remove insignificant and small regions. Next, we filter the pixel intensities using the threshold parameter th. After these preliminary steps, the resulting image undergoes thresholding. In this step, we compare the intensity of each pixel with the provided threshold value, th. If the intensity is greater than or equal to th, we classify the pixel as a part of the active region. The value of the th parameter was determined empirically based on experimental observations. For the given solar image dataset, we adjusted this parameter value to 180. After thresholding, the resulting image is subjected to common morphological operations, such as erosion and dilation.

The erosion operation eliminates small, isolated objects, also known as "islands", leaving only significant objects in the image. On the other hand, the dilation operation enhances the visibility of objects and fills small holes within them. By applying these two types of morphological operations, we are able to enhance the important features of active regions. Further information about morphological operations can be found in [10] or [24].

Figure 1 illustrates the results of the active region detection process. The applied operations successfully identify the active regions in the solar image. The precise detection of these regions, including their location and shape, is crucial for predicting Coronal Mass Ejections (CME) and solar flares.

ICCS Camera Ready Version 2024
To cite this paper please use the final published version:
DOI: 10.1007/978-3-031-63749-0_8

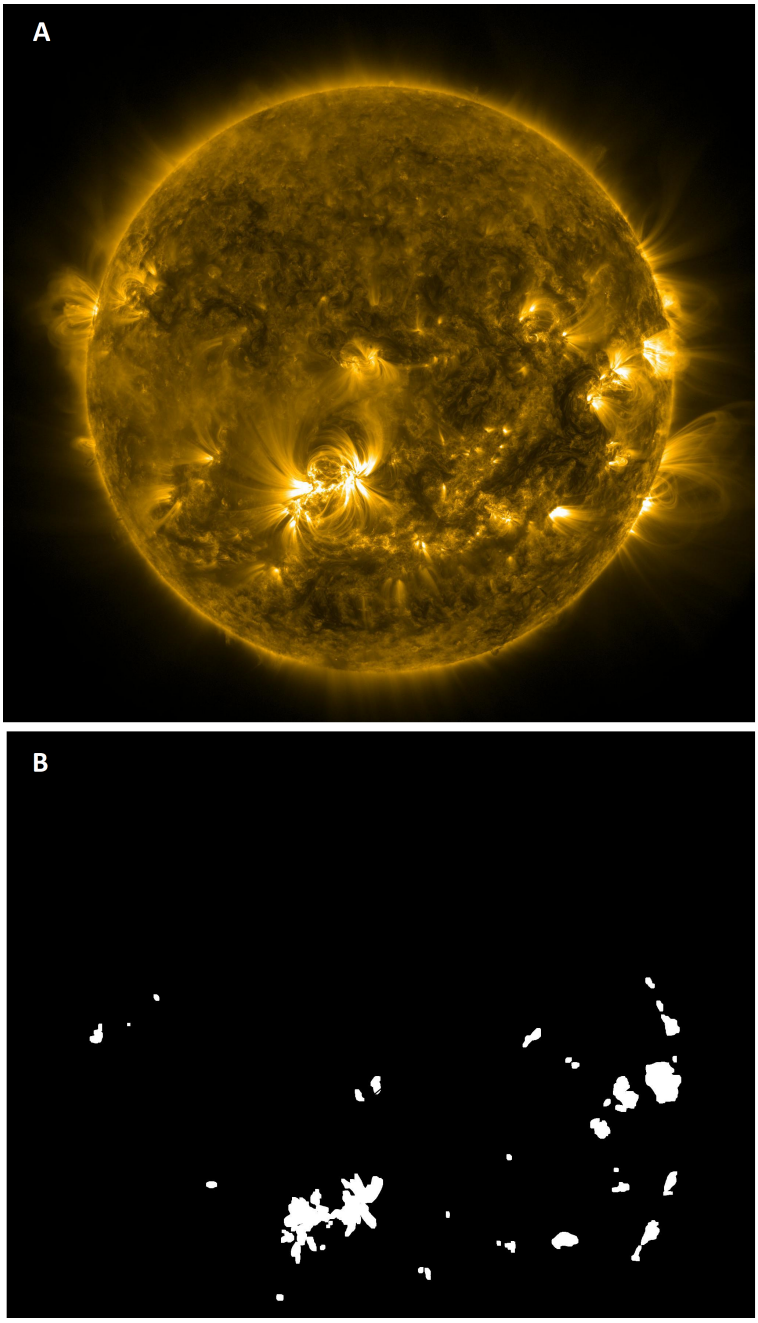

Fig. 1. Active region detection process. The top image (A) is the input image obtained from SDO Web API. The bottom image (B) is the output image obtained based on active region detection process.

ICCS Camera Ready Version 2024
To cite this paper please use the final published version:
DOI: 10.1007/978-3-031-63749-0_8

After obtaining the active regions through the previous steps, the next step involves representing them mathematically in the form of a descriptor. Since the dataset used in this study provides images with a 6-minute window cadence, it is assumed that the active regions change slightly between consecutive images due to the Sun's rotation movement. Therefore, a fast image hash is proposed that is resistant to small changes in perspective. To efficiently represent the shape and position of Active Regions on the Active Region Image (ARI), we propose a novel approach. We divide ARI into sectors (similarly to pizza slices) and calculate the sum of pixels for each sector. This method is efficient and allows for a compact representation of the shape and position of Active Regions, avoiding the need to compare high-resolution images. In order to describe the method in more detail, we begin by setting the coordinates of the image center, which we denote as cc. The radius r is fixed since the Sun's position on the image remains constant. Empirical experiments have led us to determine that the angle of $\theta = 30°$ yields optimal results. Then we need to divide the radius r to a number of layers of our descriptor. We used radius segment parameter rs for this purpose. The value of the rs can vary which has the significant impact on the descriptor. In Fig. 2 we divided the radius r only for four layers, in order to present the process transparently. After the extensive research we determined that the most optimal is to divide the radius on 10 segments. Then, we apply a cropping operation on the obtained sectors using the algorithm provided in Alg. 1. To calculate the arc points of the slice (sector) aps and ape, we use the following formulas:

$$ape_x = cc_x - 1.5 * rs * \sin\theta, \tag{1}$$

$$ape_y = cc_y - 1.5 * rs * \cos\theta, \tag{2}$$

The arc points of the sector are calculated using the formulas that involve the trigonometric functions sin and cos. These formulas calculate the row and column coordinates of two points on the arc. To extend the arc slightly beyond the circle's radius, a factor of 1.5 is applied. The obtained arc points are then used to crop the slice from ARI. The cc is circle center position thus cc_x and cc_y are center position coordinates. The procedure for slicing the ARI is repeated for each layer circle sector, resulting in a list of ARI layer sectors (CARI) which contains a list of active region pixels for every CARI. In order to obtain the mathematical description of ARI we build an active region pixels histogram assigned to given circle sector histogram (LCSH). Next, the obtained histograms are concatenated into a single vector (**DV**). The entire process is illustrated in Figure 2.

The initial step involves applying morphological operations of erosion and dilation, followed by thresholding of the input image, resulting in an image of detected active regions, as defined by Equation 3. Subsequently, the image is sliced into layer circle sectors which allows us to obtain the CARI slices, using Equation 4. In the next step the LCSH histograms are calculated, based on previously obtained CARI slices. Afterwards, we concatenate the histograms into the vector **DV**. This vector is later referred as LSBD – Layer-sector-based Descriptor.

ICCS Camera Ready Version 2024
To cite this paper please use the final published version:
DOI: 10.1007/978-3-031-63749-0_8

INPUT: ARI - active region image
rs - radius segment
cc - center coordinates of ARI
θ - angle of the slice
Local Variables:
MC - mask circle matrix
$MARI$ - mask ARI matrix
ape - coordinates of starting point on the arc
OUTPUT: $CARI$ - cropped slice of ARI
$MC := CreateBooleanCircleMatrix(cc, rs)$
$MARI := CreatePolygonMatrix([cc_x, aps_x, ape_x, cc_x],$
$[cc_y, aps_y, ape_y, cc_y])$
$CARI := CombineMasks(MC, MARI)$

Algorithm 1: Algorithm for cropping the ARI slice.

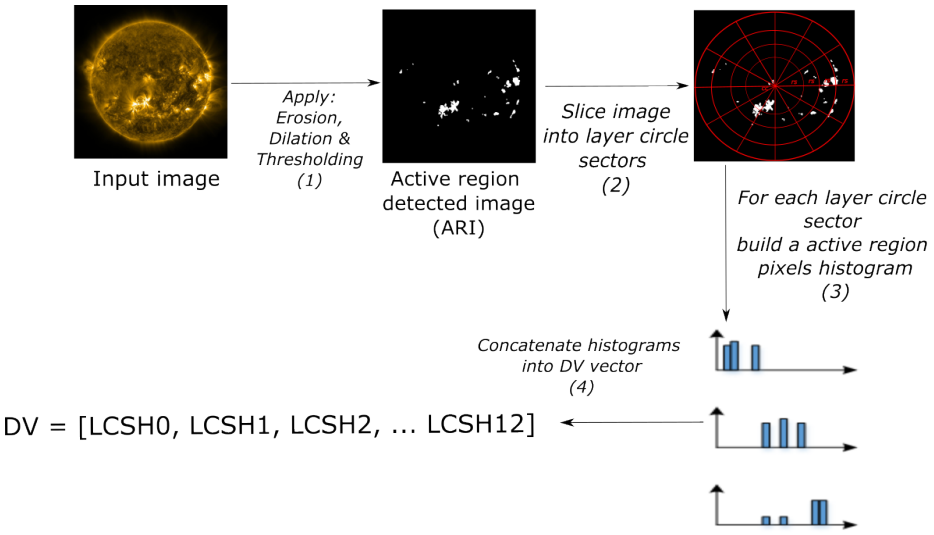

Fig. 2. Steps for calculating the layer circle sector vector (DV).

$$t(ARI, i, j, th) = \begin{cases} 1, & ARI_{i,j} \geq th \\ 0, & \text{otherwise} \end{cases}, \tag{3}$$

where th is the threshold value and ARI is the active region image.

$$\begin{aligned} &\mathbf{CI}(CARI, th)_{k,l} = \\ &= \sum_{i=k*ssx}^{(k+1)*ssx-1} \sum_{j=l*ssy}^{(l+1)*ssy-1} t(CARI, i, j, th) \end{aligned}, \tag{4}$$

where ssx is the sector size in x-axis and ssy is the sector size in y-axis. The Layer-sector-based Descriptor (LSBD) calculation process serves to significantly reduce the data volume during the encoding stage. The primary objective of this

ICCS Camera Ready Version 2024
To cite this paper please use the final published version:
DOI: 10.1007/978-3-031-63749-0_8

Table 1. Tabular representation of the fully-connected autoencoder model.

Layer (type)	Output	Filters (in, out)	Params
$Input(InputLayer)$	[1, 120]		0
$Linear\_1(Linear)$	[1, 60]	120, 60	7,260
$ReLU\_1$	[1, 60]	0	
$Linear\_2(Linear)$	[1, 60]	60, 30	1,830
$ReLU\_2$	[1, 30]	0	
$Encoded(latent-space)$	[1, 30]		
$Linear\_4(Linear)$	[1, 30]	30, 60	1,860
$ReLU\_4$	[1, 60]	0	
$Linear\_5(Linear)$	[1, 120]	60, 120	7,320
$ReLU\_5$	[1, 120]	0	
$Decoded(Tanh)$	[1, 120]		

process is to generate an intermediate, hand-crafted mathematical representation of AR images that can be utilized in the subsequent step. Thanks to this process we obtained the LSBD of 120-length (12 sectors and 10 layers), which is a significant reduction in comparison to the full-disc image. Despite that, we can reduce it even further, by using the fully-connected autoencoder described in Sec. 3.2.

3.2 Hash Generation

This section details the process of generating a hash using a Layer-sector-based Descriptor (LSBD) as input. The objective of this step is to produce a representative hash that accurately describes the solar image, with a particular focus on its active regions at a specific timestamp. This step is critical as it enables the reduction of data during the retrieval stage, as discussed in Section 3.3. To execute this operation, we employed a fully-connected autoencoder (AE) to encode the acquired LSBD. Autoencoders are utilized in various machine learning tasks, including image compression, dimensionality reduction, feature extraction, and image reconstruction [7, 11, 22]. Autoencoders are ideal for generating semantic hashes as they utilize unsupervised learning. The architecture of the autoencoder model is presented in Table 1, and it should be analyzed from top to bottom. As illustrated, the model is relatively straightforward yet effective in reducing the hash length without significant information loss regarding magnetic regions of the magnetogram. It is worth noting that only the encoded portion of the trained AE's latent space is used for hash generation, while the decoding portion of the AE is solely utilized for training purposes. After conducting several experiments, we concluded that 40 epochs are adequate to achieve a satisfactory level of generalization without experiencing overfitting.

Table 1 demonstrates the utilization of a convolutional autoencoder for generating hashes, with the top layer serving as input. A one-dimensional autoen-

ICCS Camera Ready Version 2024
To cite this paper please use the final published version:
DOI: 10.1007/978-3-031-63749-0_8

coder was utilized due to the fact that magnetic intensity descriptors are one-dimensional vectors, which helps to minimize computational complexity. By using this process, we are able to effectively reduce the hash length while retaining a substantial amount of information about the active regions of the solar image. The mean squared error function was employed as the loss function, and we determined that training the model for 40 epochs was sufficient for achieving the required level of generalization and avoiding network over-fitting. After the training process, each image descriptor was passed through the encoding layers of the autoencoder, resulting in a 30-element hash called the Layer-Sector Solar Hash (LSSH). This hash can be utilized in content-based retrieval applications that involve solar images. Furthermore, the selected autoencoder architecture was deliberately chosen to ensure optimal generalization.

3.3 Retrieval

In the final phase of the proposed method, we use the previously generated hashes for solar image retrieval. After completing the previous steps, we assume that each solar image in our database has been assigned a hash. The retrieval process involves executing an image query by comparing the distances between the hash of the query image and the hashes created for all images stored in the dataset. To perform this retrieval, we need to have a database of solar images that have undergone hash generation. In the subsequent step, we compute the distance (d) between the hash of the query image and every hash in the database. For this purpose, the cosine distance measure is employed. (see [13] for additional information).

$$\cos(QH_j, IH_j) = \sum_{j=0}^{n} \frac{(QH_j \bullet IH_j)}{\|QH_j\| \, \|IH_j\|}, \tag{5}$$

where $\bullet$ is a dot product, QH_j is the query image hash, and IH_j a consecutive image hash. After computing the cosine distance, the images in the database are sorted in ascending order based on their distance from the query hash. In the final step of the proposed method, the n images closest to the query are retrieved and returned to the user. The value of the parameter n needs to be provided by the user to execute the query. Alg. 4 illustrates the complete process as pseudo-code. An alternative method for image retrieval involves setting a threshold for the cosine distance. In this approach, the user provides a threshold parameter instead of n, and images are retrieved if their cosine distance to the query is below the threshold. The presented technique can also support the threshold-based image retrieval method, where images are retrieved if their cosine distance to the query is below the threshold value. However, the first method, which retrieves the top n images closest to the query, is more user-friendly and recommended. The retrieval process is presented in Alg. 2.

ICCS Camera Ready Version 2024
To cite this paper please use the final published version:
DOI: 10.1007/978-3-031-63749-0_8

INPUT: $ImageHashes$, $QueryImage$, n
OUTPUT: $RetrievedImages$
foreach $ImageHash \in ImageHashes$ **do**
  $QueryImageHash = CalculateHash(QueryImage)$
  $D[i] = Cos(QueryImageHash, ImageHash)$
end
$SortedDistances = SortAscending(D)$
$RetrievedImages = TakeFirst(n)$

Algorithm 2: Image retrieval steps.

4 Experimental Results

In this section, we present the simulation results and a solution for evaluating unlabeled images using unsupervised learning for encoding descriptors. The lack of labeled data necessitated the use of this approach. As there was a lack of labeled data, evaluating the proposed method against state-of-the-art approaches was difficult. To overcome this issue, we utilized the rotation movement of the Sun to identify a set of similar images (SI). We speculated that consecutive images taken within a small-time window would display similar active regions, albeit with minor displacements. The solar images provided were captured at 6-minute intervals, which implied that they were similar due to the Sun's movement. The only necessary adjustment was to vary the time window. After experimentation, we found that images captured within a 48-hour time window could be considered similar. Let us analyze the following case. Suppose we have an image captured at 2011-02-15, 00:00:00. According to the assumptions mentioned earlier, we can consider every image captured 24 hours before and after as similar. To identify images, we use their timestamps solely for evaluation purposes. Table 2 presents the process of determining similar images. A set of experiments was conducted to assess image similarity using the proposed method. Each experiment comprised the following steps:

1. Execute an image query to retrieve images.
2. Comparing the retrieved images' timestamps with the query image timestamp.
3. Identifying images with timestamps that fell within a 48-hour window as similar to the query.

After defining the set of similar images (SI), we can define the performance measures of precision and recall [8, 25] based on the following sets:

- SI - set of similar images,
- RI - set of retrieved images for query,
- $PRI(TP)$ - set of positive retrieved images (true positive),
- $FPRI(FP)$ - false positive retrieved images (false positive),
- $PNRI(FN)$ - positive, not retrieved images,
- $FNRI(TN)$ - false, not retrieved images (TN).

ICCS Camera Ready Version 2024
To cite this paper please use the final published version:
DOI: 10.1007/978-3-031-63749-0_8

Table 2. Defining image similarity. Based on experiments, we determined that images within a 48-hour window can be treated as similar. This allows to evaluate the method.

Timestamp	SI (similar image)/ NSI (not similar image)
2011-02-13, 23:54:00	NSI
2011-02-14, 00:00:00	SI
2011-02-14, 00:06:00	SI
2011-02-14, 00:12:00	SI
2011-02-14, 00:18:00	SI
2011-02-14, 00:24:00	SI
2011-02-14, 00:30:00	SI
.....	SI
2011-02-15, 00:00:00	QI (query image)
.....	SI
2011-02-15, 23:24:00	SI
2011-02-15, 23:30:00	SI
2011-02-15, 23:36:00	SI
2011-02-15, 23:42:00	SI
2011-02-15, 23:48:00	SI
2011-02-15, 23:54:00	SI
2011-02-16, 00:00:00	NSI

We can then define the measures of precision, recall and F_1 for CBIR systems.

$$precision = \frac{|PRI|}{|PRI + FPRI|}, \tag{6}$$

$$recall = \frac{|PRI|}{|PRI + PNRI|}. \tag{7}$$

$$F_1 = 2\frac{precision \cdot recall}{precision + recall}. \tag{8}$$

The experimental results presented in Tab. 3 are promising, as demonstrated by the average value of F_1 and the high precision values. Our method demonstrated superior performance compared to previous works, with an average precision of 0.92186. In comparison, Banda et al. achieved a precision of 0.848, and Angryk et al. achieved a precision of 0.850 [3, 5]. Moreover, our method also outperformed the results obtained in the study by Grycuk et al. [12]. Most of the solar images that had a small distance from the query image were retrieved successfully. However, for solar images with larger distances, they were classified as positive but not retrieved images ($PNRI$). Nevertheless, this value was considerably reduced compared to previous studies. The high values of $PNRI$ can be attributed to the Sun's rotation movement, which may cause active regions to shift or disappear, even within the 48-hour time window.

ICCS Camera Ready Version 2024
To cite this paper please use the final published version:
DOI: 10.1007/978-3-031-63749-0_8

Table 3. Experiment results for the proposed algorithm. Due to lack of space, we present only a part of all queries.

Timestamp	RI	SI	PRI(TP)	FPRI(FP)	PNRI(FN)	Prec.	Recall	F_1
2011-01-01 00:00:00	199	241	187	12	54	0.94	0.78	0.85
2011-01-04 16:06:00	403	481	384	19	97	0.95	0.80	0.87
2011-01-06 19:12:00	412	481	366	46	115	0.89	0.76	0.82
...								
2011-01-15 18:18:00	386	481	361	25	120	0.94	0.75	0.83
2011-01-18 02:24:00	430	481	389	41	92	0.90	0.81	0.85
2011-01-20 12:24:00	404	481	379	25	102	0.94	0.79	0.86
...								
2011-02-03 07:36:00	404	481	373	31	108	0.92	0.78	0.84
2011-02-05 19:42:00	419	481	368	51	113	0.88	0.77	0.82
2011-02-13 17:48:00	420	481	387	33	94	0.92	0.80	0.86
Avg.						**0.922**	**0.788**	**0.849**

5 Conclusions

We presented a new approach for very fast retrieving and classifying solar images using sector-based image hashing. Our initial attempt was to generate hashes directly from full-disc images, but we encountered computational complexity issues due to too large input data for the autoencoder. Consequently, we opted to create intermediate hand-crafted features to address this challenge. We utilized morphological operations to preprocess input images and detect active regions. Next, we compute the layer-sector-based descriptors. Once this step is completed, we employ a fully-connected autoencoder to encode the descriptors, resulting in the concise Layer-Sector Solar Hash. By undergoing a second encoding process, we are able to greatly reduce the length of the descriptors. Our experiments have shown a reduction of over four times compared to the layer-sector-based descriptor obtained in the initial stage. This reduction in hash length is crucial for improving the speed of calculating the distances between hashes, which in turn determines the similarity of solar images. Since solar AIA (Atmospheric Imaging Assembly) images are not labeled, we consider images produced within a short time frame of each other (typically up to several hours) to be similar. In reality, even at different times, the Sun's configuration may be similar. Hence, our precision and recall measures, which depend solely on the image content, are likely to have even higher values in practical use. The approach we have presented has several potential applications, including searching, classifying, and retrieving solar flares, which are of critical importance for many aspects of life on Earth.

References

1. Banda, J., Angryk, R., Martens, P.: Steps toward a large-scale solar image data analysis to differentiate solar phenomena. Solar Physics **288**(1), 435–462 (2013)

ICCS Camera Ready Version 2024
To cite this paper please use the final published version:
DOI: 10.1007/978-3-031-63749-0_8

2. Banda, J.M., Angryk, R.A.: Selection of image parameters as the first step towards creating a cbir system for the solar dynamics observatory. In: 2010 International Conference on Digital Image Computing: Techniques and Applications. pp. 528–534. IEEE (2010)
3. Banda, J.M., Angryk, R.A.: Large-scale region-based multimedia retrieval for solar images. In: International Conference on Artificial Intelligence and Soft Computing. pp. 649–661. Springer (2014)
4. Banda, J.M., Angryk, R.A.: Scalable solar image retrieval with lucene. In: 2014 IEEE International Conference on Big Data (Big Data). pp. 11–17. IEEE (2014)
5. Banda, J.M., Angryk, R.A.: Regional content-based image retrieval for solar images: Traditional versus modern methods. Astronomy and computing **13**, 108–116 (2015)
6. Boubrahimi, S.F., Aydin, B., Schuh, M.A., Kempton, D., Angryk, R.A., Ma, R.: Spatiotemporal interpolation methods for solar event trajectories. The Astrophysical Journal Supplement Series **236**(1), 23 (2018)
7. Brunner, C., Kő, A., Fodor, S.: An autoencoder-enhanced stacking neural network model for increasing the performance of intrusion detection. Journal of Artificial Intelligence and Soft Computing Research **12**(2), 149–163 (2022). https://doi.org/10.2478/jaiscr-2022-0010
8. Buckland, M., Gey, F.: The relationship between recall and precision. Journal of the American society for information science **45**(1), 12 (1994)
9. Dolecki, M., Karczmarek, P., Gałka, Ł., Zawadka, M., Smolka, J., Skublewska-Paszkowska, M., Lukasik, E., Powroznik, P., Gawda, P., Czerwinski, D.: On the detection of anomalies with the use of choquet integral and their interpretability in motion capture data. In: 2022 IEEE International Conference on Fuzzy Systems (FUZZ-IEEE). pp. 1–9. IEEE (2022)
10. Dougherty, E.R.: An introduction to morphological image processing. SPIE, 1992 (1992)
11. Grycuk, R., Galkowski, T., Scherer, R., Rutkowski, L.: A novel method for solar image retrieval based on the parzen kernel estimate of the function derivative and convolutional autoencoder. In: 2022 International Joint Conference on Neural Networks (IJCNN). pp. 1–7. IEEE (2022)
12. Grycuk, R., Scherer, R.: Grid-based concise hash for solar images. In: International Conference on Computational Science. pp. 242–254. Springer (2021)
13. Kavitha, K., Rao, B.T.: Evaluation of distance measures for feature based image registration using alexnet. arXiv preprint arXiv:1907.12921 (2019)
14. Kempoton, D., Schuh, M., Angryk, R.: Towards using sparse coding in appearance models for solar event tracking. In: 2016 19th International Conference on Information Fusion (FUSION). pp. 1252–1259 (2016)
15. Kempton, D.J., Schuh, M.A., Angryk, R.A.: Describing solar images with sparse coding for similarity search. In: 2016 IEEE International Conference on Big Data (Big Data). pp. 3168–3176. IEEE (2016)
16. Kempton, D.J., Schuh, M.A., Angryk, R.A.: Tracking solar phenomena from the sdo. The Astrophysical Journal **869**(1), 54 (2018)
17. Kiersztyn, A., Karczmarek, P., Kiersztyn, K., Pedrycz, W.: The concept of detecting and classifying anomalies in large data sets on a basis of information granules. In: 2020 IEEE International Conference on Fuzzy Systems (FUZZ-IEEE). pp. 1–7. IEEE (2020)
18. Krizhevsky, A., Hinton, G.E.: Using very deep autoencoders for content-based image retrieval. In: ESANN. vol. 1, p. 2 (2011)

ICCS Camera Ready Version 2024
To cite this paper please use the final published version:
DOI: 10.1007/978-3-031-63749-0_8

19. Kucuk, A., Banda, J.M., Angryk, R.A.: A large-scale solar dynamics observatory image dataset for computer vision applications. Scientific data **4**, 170096 (2017)
20. Ma, R., Boubrahimi, S.F., Hamdi, S.M., Angryk, R.A.: Solar flare prediction using multivariate time series decision trees. In: 2017 IEEE International Conference on Big Data (Big Data). pp. 2569–2578. IEEE (2017)
21. Mairal, J., Bach, F., Ponce, J., Sapiro, G.: Online learning for matrix factorization and sparse coding. Journal of Machine Learning Research **11**(Jan), 19–60 (2010)
22. Najgebauer, P., Scherer, R., Rutkowski, L.: Fully convolutional network for removing dct artefacts from images. In: 2020 International Joint Conference on Neural Networks (IJCNN). pp. 1–8. IEEE (2020)
23. Salakhutdinov, R., Hinton, G.: Semantic hashing. International Journal of Approximate Reasoning **50**(7), 969 – 978 (2009). https://doi.org/https://doi.org/10.1016/j.ijar.2008.11.006, http://www.sciencedirect.com/science/article/pii/S0888613X08001813, special Section on Graphical Models and Information Retrieval
24. Serra, J.: Image analysis and mathematical morphology. Academic Press, Inc. (1983)
25. Ting, K.M.: Precision and recall. In: Encyclopedia of machine learning, pp. 781–781. Springer (2011)

ICCS Camera Ready Version 2024
To cite this paper please use the final published version:
DOI: 10.1007/978-3-031-63749-0_8